Farm-level Interactions Study of a Novel Tri-port Soft-switching Medium-Voltage String Inverter (MVSI) based Large-scale PV-Plus-Storage Farms

Vikram Roy Chowdhury, Zheng An, Rajendra Prasad Kandula and Deepak Divan
School of Electrical and Computer Engineering
Georgia Institute of Technology
Atlanta, GA 30332 USA
vchowdhury6@gatech.edu

***Abstract*—A medium-voltage photovoltaic power conversion unit supported by battery based on a novel topology of soft switching solid state transformer is presented in this paper. It can reduce the Levelized Cost of Energy (LCOE) of PVS farm in an extended degree. However, its capability to provide grid-support services, such as frequency response, reactive power support, etc, have not been demonstrated. A series/parallel combination of these modules form a large 20 MVA solar farm. To validate them with reduced computation burden, a small-signal model of MVSI is firstly derived and validated in this paper. The model has been validated to match the full-switch model in both steady-state and dynamic conditions. Next, a farm-level simulation based on the proved small-signal model was implemented to demonstrate grid-support services. Real irradiation date from NREL is used to show the operational capabilities of the system. The overall farm is simulated based on MATLAB/Simulink domain to check the performance for various cases namely: power transfer from dc-ac side, reactive power support during grid voltage sag and utilization of battery during grid voltage disturbance or partial shading over PV panels.**

***Index Terms*—Soft switching solid state transformer ($S4T$), Small-signal modeling, Photovoltaic (PV) application, Three-phase system.**

I. Introduction

FOCUS to reduce emission due to fossil fuel, usage of renewable energy resources has become a necessity to achieve clean and green power production architecture [1]–[7]. One of the most common forms of renewable power sources is that of photo-voltaic (PV) power generation. Uncertain nature of solar irradiation causes extreme difficulty in maintaining seamless and uninterrupted power supplied to the load/grid. Therefore, a storage system becomes a necessity for such a PV generation system [8], [9]. Also, with proper storage, optimal usage of the PV system along with LCOE reduction can be accomplished as presented in [10]. Also, it becomes necessary for high power application that an isolation is provided between the generation and the transmission system. To cater this, several isolated topology of solid state transformers have been reported [11], [12]. One of the most recent works for an isolated topology is that of soft-switching solid state transformer (S4T) [13], [14]. The topology is based on current source inverter rather traditional voltage source type converter. Also, the S4T is required to achieve soft-switching for the whole range of operation. These make the control of the overall system to be challenging. Control architecture based on model predictive priority switching (MPPS) for S4T has been reported in [15]. This switching scheme calculates the most optimal switching trajectory and balances out the power in a per switching cycle basis. However, such a control architecture relies heavily on the parameter of the high frequency transformer, the magnetizing inductance to be more precise and is very heavy computationally. Also, MPPS architecture presented in literature might not provide optimal performance due to the inherent low inertia architecture of the S4T based MVSI converter. Therefore, to cater for this problem, a feed-forward compensation based MPPS for an S4T based MVSI has been presented in [16]. To mitigate this and achieve global stability, a Lyapunov energy function based analysis and control architecture has been reported in [6]. The Lyapunov energy function based control architecture for an ac-ac standalone application has been presented and several case studies are shown. However, no discussion on how the control architecture would operate under parallel connected converters with interconnecting line impedance and weak grid condition has been presented or discussed. Modular architecture and operation of a parallel connected tri-port S4T has been presented in [17]. A full switching model has been utilized for the simulation study with each converter of 25 KVA. A 300 KVA system has been designed and presented for various case studies. Such a design makes the overall simulation very slow due to low sampling time (in the order of μs). Also, on the grid, slower dynamics are of more interest to check for the synchronous stability as well as any initiated resonance oscillation due to the output CL filter. Although, it can reduce LCOE to a great extent as demonstrated in [10], however, grid support services should be accomplished with reduced computational effort. To cater the above issues, small-signal model averaged over a switching cycle has been utilized in this paper where each state variable is averaged over a switching cycle. This type of a model ensures the simulation is much faster and therefore, can analyze a bigger system at the utility level (20 MVA in this case). A series/parallel combination of

This work was carried out at the Center for Distributed Energy, Georgia Institute of Technology. This work is sponsored by Solar Energy Technologies Office (SETO) of Department of Energy (DoE) under the award number DE-EE0008351.

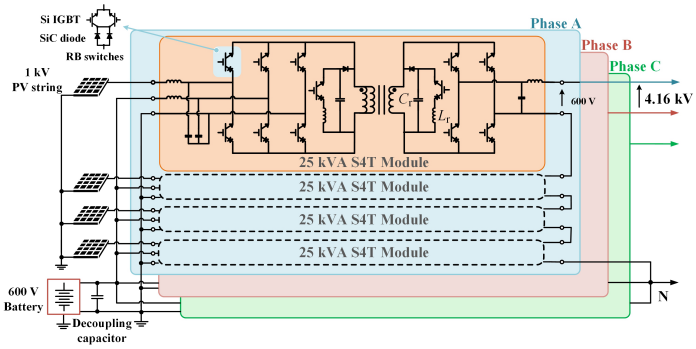

Fig. 1: Simplified circuit schematic of a tri-port $MVSI$

each modular converter of 25 KVA is accomplished to build the 20 MVA system. All the interconnecting impedance in between the connecting lines are considered along with the grid impedance to emulate a weak grid. Using these non-idealities and using real PV irradiation data from the NREL data port [18], the overall system is simulated for a 20 MVA PV farm and several case study results are presented. The rest of the paper is organized as follows: section II has two subsections: subsection A summarizes the overall architecture of each unit of the tri-port MVSI and the need, utilization and verification of the small-signal model with the full switching model, subsection B presents the step by step development of the 20 MVA PV farm with the small-signal units as the building blocks, section III presents the simulation results for various important case studies for a 20 MVA PV farm followed by conclusion in section IV.

II. Tri-Port MVSI

In this paper, a 300 KVA tri-port MVSI has been considered as the building block for the overall system as presented in Fig. 1. Each one of these 300 KVA units are made up of 25 KVA S4T modules connected in a series parallel combination in each of the ports (dc or ac). A common storage/capacitor is connected across all the modules, where the decoupling capacitor is required to eliminate double-line frequency pulsating power for single-phase ac output but not for the three-phase system. Besides, the common storage/capacitor allows the power exchange across all modules, which guarantees a balanced output across the series connected modules even under unbalanced inputs. Storage is not necessary for converter operation and can be replaced by a small film capacitor, called the decoupling capacitor, necessary to eliminate double-line frequency pulsating power for single phase AC applications. The size of the decoupling capacitor can be reduced dramatically for a balanced three-phase system. In addition, the common battery/capacitor allows the exchange of power across the modules, guaranteeing a balanced output across the series-connected modules even under unbalanced input conditions such as partial shading and PV module mismatches [17]. The next subsection presents the need, utilization and verification of the small-signal model with the full switching model for the 25 KVA tri-port S4T converter module.

A. Small-Signal Modeling of tri-port MVSI

In this section, the small-signal model verification with the switching model of the tri-port MVSI has been presented for various states of the system. As mentioned in the previous sections, using switching averaged small-signal model over the full switching model for each 25 KVA module makes the simulation of the PV farm not only faster but also feasible. Just to understand in a quantitative form, one module of 25 KVA with detailed switching model takes approximately 10 minutes to complete 10 line cycles i.e. 0.167 sec whereas the average model for the same time requires less than a minute to complete 10 line cycle of simulation. From these quantification it can be very well concluded that as the system is scaled up there will be significant advantage in terms of simulation time using an average model. A single-phase full switching model of a tri-port S4T is presented in Fig. 2. Averaging the quantities of each port of Fig. 2 i.e. voltage, current, the small-signal model has been accomplished. The step by step derivation of the small-signal equivalent circuit of Fig. 3 is briefly presented in this section. For the PV port from Fig. 3 the dynamics of the circuit are given by

$$\begin{aligned} L_{PV}\frac{di_{LPV}}{dt} &= v_{PV} - v_{cPV} \\ C_{PV}\frac{dv_{cPV}}{dt} &= i_{LPV} - d_{PV}i_m \end{aligned} \tag{1}$$

where $L_{PV} = L^{dc}$ is the inductance of the PV side, $C_{PV} = C^{dc}$ is the capacitor for the PV side, i_{LPV} is the PV side inductor current for the PV port and v_{cPV} is the PV port capacitor voltage, d_{PV} is the duty ratio for which the PV is supplying power to the system and i_m is the magnetizing current. Similarly, for the battery port the dynamics are given by

$$\begin{aligned} L_{bat}\frac{di_{Lbat}}{dt} &= v_{bat} - v_{cbat} \\ C_{bat}\frac{dv_{cbat}}{dt} &= i_{Lbat} - d_{bat}i_m \end{aligned} \tag{2}$$

where $L_{bat} = L^{dc}$ is the inductance of the battery side, $C_{PV} = C^{dc}$ is the capacitor for the battery side, i_{Lbat} is the battery side inductor current for the battery port and v_{cbat} is the battery port capacitor voltage and d_{bat} is the duty ratio for which the battery is either getting charged or discharged depending on the requirement. The dynamics of the ac side of the tri-port MVSI are given by

$$\begin{aligned} C_{grid}\frac{dv_{cgrid}}{dt} &= d_{ac}i_m - i_{load/grid} \\ L_{grid}\frac{di_{Lgrid}}{dt} &= v_{cgrid} - v_{ac} \end{aligned} \tag{3}$$

where $C_{grid} = C^{ac}$ is the ac side capacitor, $L_{grid} = L^{ac}$ is the ac side inductor, v_{cgrid} is the capacitor voltage for the ac side, d_{ac} is the duty ratio for which the ac side is connected to the secondary of the high frequency transformer, $i_{load/grid}$ is the ac side load or grid current and v_{ac} is the load or grid voltage. Finally, the dynamics of the magnetization branch is given by

$$L_m\frac{di_m}{dt} = d_{PV}v_{cPV} + d_{bat}v_{cbat} - d_{ac}v_{cgrid} \tag{4}$$

where L_m is the magnetization inductance, i_m is the magnetizing current. To accomplish a small-signal model, the small-signal changes of each of the variables of these dynamic equations are used i.e. $d_{PV} = D_{PV} + \Delta d_{PV}$ where D_{PV} is the

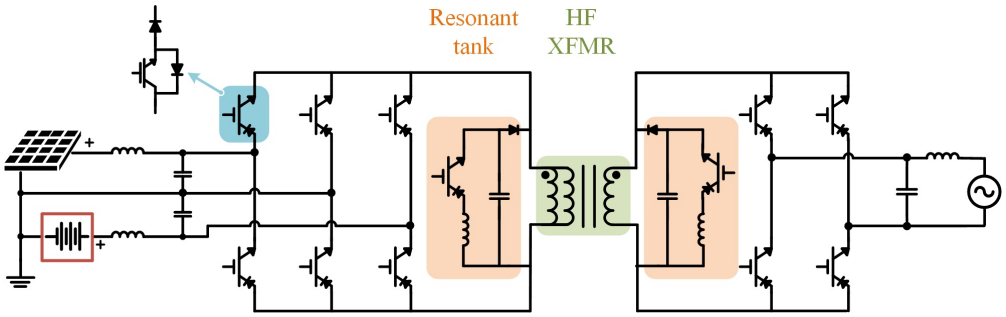

Fig. 2: Simplified equivalent circuit for 25 KVA tri-port MVSI module

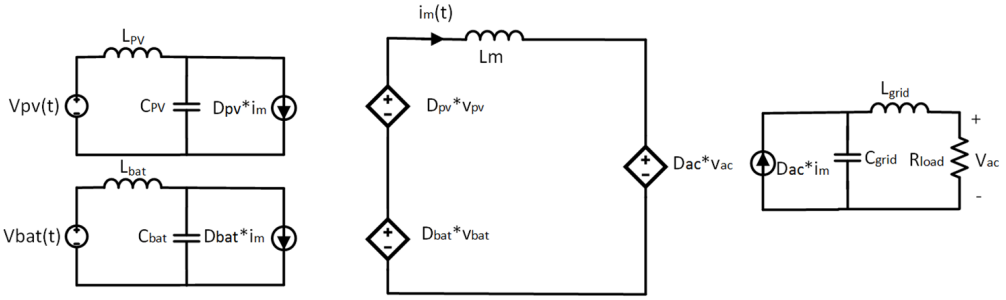

Fig. 3: Simplified equivalent small-signal circuit model for a 25 KVA tri-port MVSI module

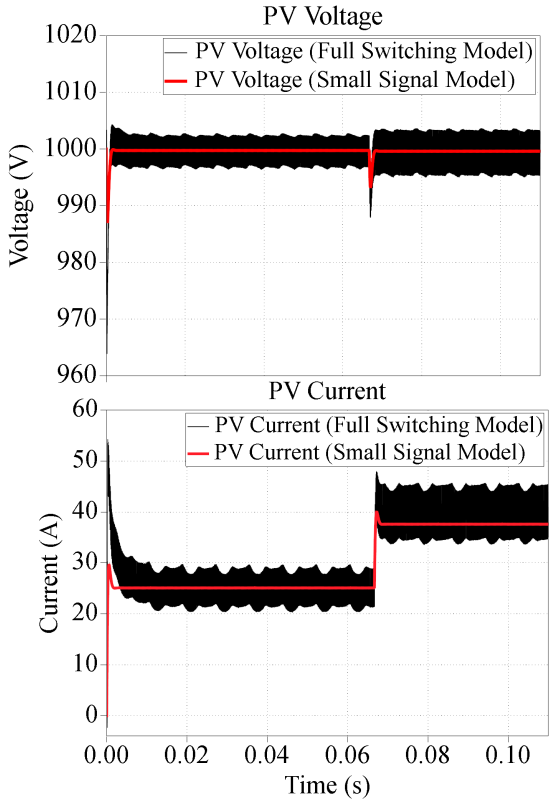

Fig. 4: PV voltage and current during a step change in the load on the ac port

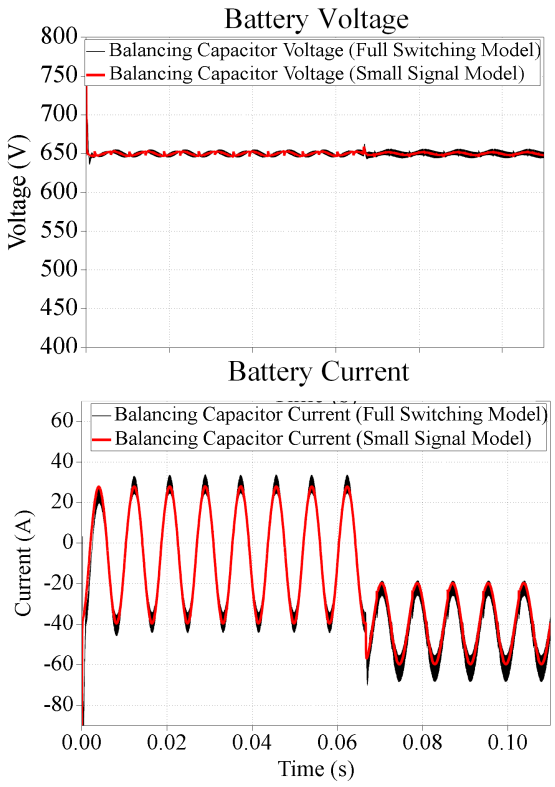

Fig. 5: Battery port voltage and current during step change in load on ac port

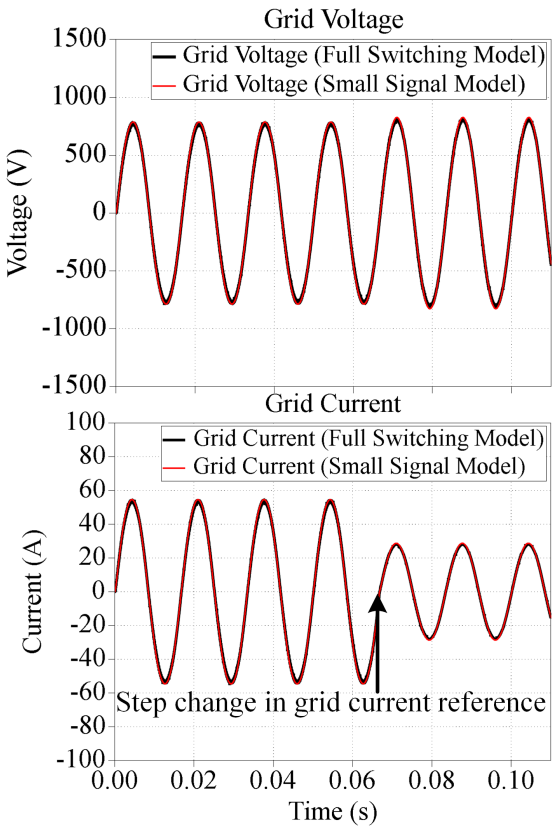

Fig. 6: Voltage and current of the ac port during step change in the load

steady state value and Δd_{PV} is the small signal change. Similarly, $d_{bat} = D_{bat} + \Delta d_{bat}$ and $d_{ac} = D_{ac} + \Delta d_{ac}$. Also, $i_m = I_m + \Delta i_m$, $i_{LPV} = I_{LPV} + \Delta i_{LPV}$, $i_{Lbat} = I_{Lbat} + \Delta i_{Lbat}$. Finally, for the capacitor voltages, $v_{cPV} = V_{cPV} + \Delta v_{cPV}$, $v_{cbat} = V_{cbat} + \Delta v_{cbat}$ and $v_{cgrid} = V_{cgrid} + \Delta v_{cgrid}$. Using these definitions and substituting in (1) through (4) the equivalent small-signal model of the tri-port MVSI of Fig. 1) is obtained. To verify the accuracy of the derived small-signal model, the full switching model and the small-signal circuit model are simulated via MATLAB/Simulink and PLECS domain for a 25 KVA system to verify the operation of the system. The parameters for the simulation are: magnetizing inductance $L_m = 350\mu H$, PV voltage of 1000 V, battery voltage of 650 V and rms ac voltage of 600 V. The filter parameters are $C_{pv} = C_{bat} = C_{grid} = 50\mu F$, $L_{pv} = L_{bat} = L_{grid} = 0.5mH$ and the magnetizing current reference is $I_m^{ref} = 110A$. Using these parameters, the 25 KVA module is simulated along with the full switching model and various results are obtained. The PV and battery ports' voltage and current during the load step change are presented respectively in Figs. 4 and 5. Finally, the result during the step change on the ac port is presented in Fig. 6. From these results it is observed that the full switching model can be replaced by its equivalent small-signal model and all transients of the system other than the switching transient can be observed. Therefore, without loss of generality for the farm level simulation, the full switching model is replaced by its

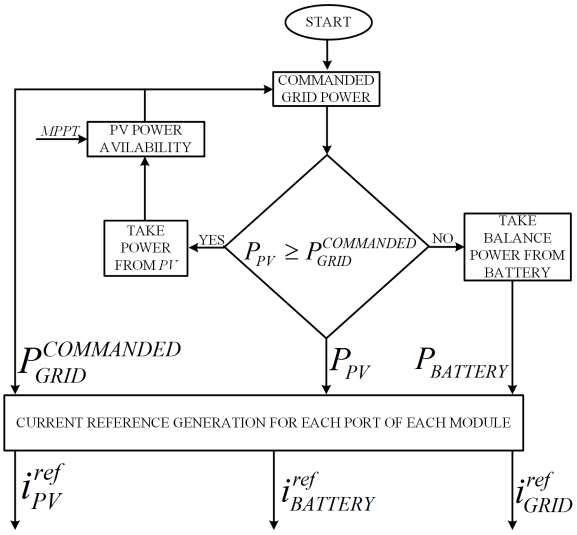

Fig. 7: Flow chart of the overall control philosophy for the 20 MVA PV farm

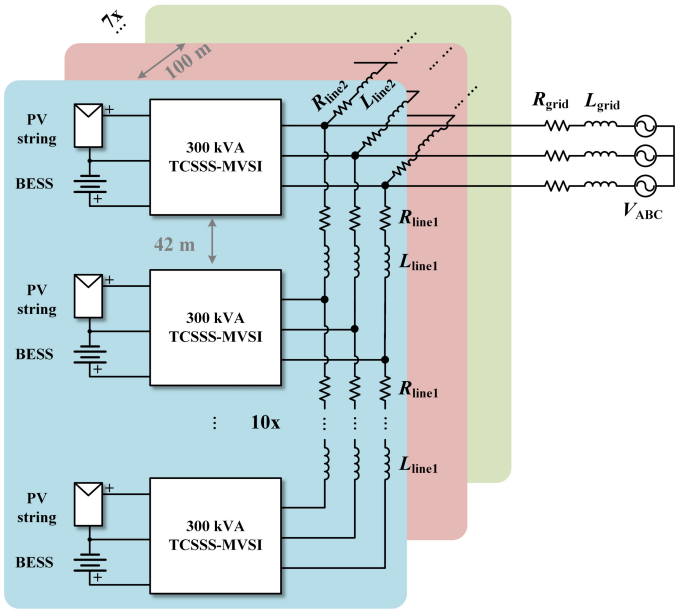

Fig. 8: Simplified schematic diagram of the 20 MVA PV farm

equivalent small-signal model and various case study results are obtained. The next section presents the simulation results for the 20 MVA PV farm showing several important case study results to realize the feasibility and performance of the overall system.

B. Step by step development for 20 MVA PV Farm

The simplified circuit schematic presented in Fig. 1 is replaced by its equivalent small-signal model to ensure faster simulation speed and each unit of 300 KVA is utilized as the building block for a 20 MVA PV farm as presented in Fig. 8. A series/parallel combination of each of these modules are carried out to accomplish the 20 MVA PV farm design. The

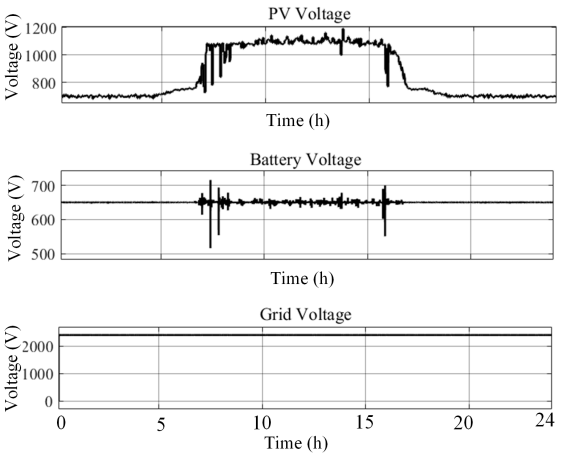

Fig. 9: Voltages at various ports for the tr-port $S4T$

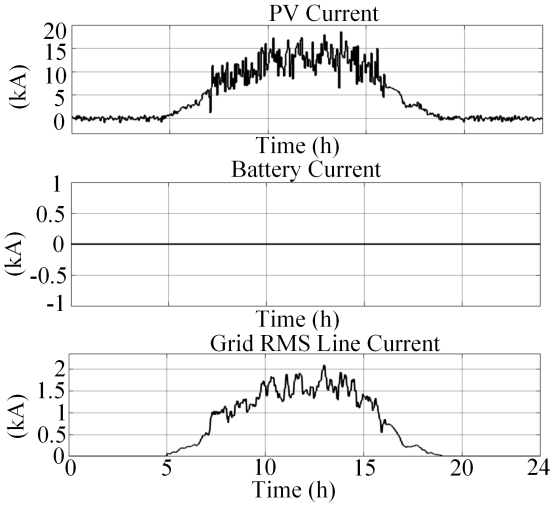

Fig. 10: Currents at various ports of the tri-port MVSI without the battery smoothing

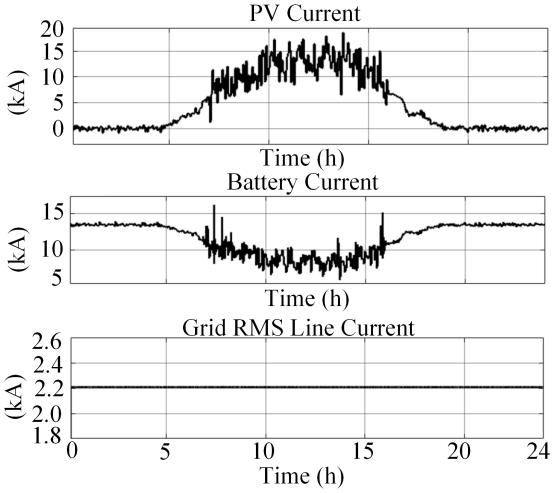

Fig. 11: Currents at various ports of the tri-port MVSI with the battery smoothing

overall control philosophy has been presented in form of a flowchart in Fig. 7. In Fig. 8, to emulate the physical distance between each 300 KVA module, (i.e. twelve 25 KVA units of Fig. 1) interconnecting impedance of R_{int} and L_{int} are connected whose values are presented in section III (simulation results). Also, the grid is considered to be non-ideal i.e. weak and therefore, grid impedance (R_{grid} and L_{grid}) are connected, whose values are also presented in section III. The overall simplified philosophy of control for the PV farm is summarized as:

- Major objective is to transfer power to the grid if sufficient PV power is available.
- Else, transfer the balance power from the battery, If PV power is more than the grid schedule utilize the balance power to charge the battery.
- Finally, achieve reactive power support during grid voltage sag.

With these objectives, the overall control architecture has been developed. The top level controller commands the power to be extracted from each ports of the each of the modules. The lower level controller generates the current references from each port of each of the modules so that power balance can be achieved at the module level. Another major objective of the lower level controller is to maintain the magnetizing current of each high frequency transformer at its reference value. The next section presents the verification the PV farm using these small-signal units via computer simulation based on MATLAB/Simulink for various important case studies.

III. Simulation Results

The PV farm presented in Fig. 8, is modeled and simulated based on MATLAB/Simulink domain and the various case study results are presented and discussed this section. These are:

- Operation under partial shading condition for the MVSI.
- Reactive power support during unsymmetrical voltage sag
- Operation with grid voltage harmonics.

To achieve more realistic results, the PV irradiation is extracted from NREL data port [18] for 24 hrs. However, the overall data for a day is time compressed to 2.4 sec and the performance of the overall system with variation in the solar irradiation profile is obtained. The model of the single PV panel used for this work is SunPower-305WHT. The interconnecting wires are constructed with 500 MCM aluminum overhead line with the distance between each unit of approximately 42 metres. The unit impedance for the interconnecting lines are therefore set to $0.014m\Omega/m$ and $200nH/m$ [19]. The grid impedance is set to 5% of the base impedance of the overall system and is set to $R_{grid} = 4.5m\Omega$ and $L_{grid} = 112\mu H$. The result showing the voltage of various ports (PV, battery and grid) is presented in Fig. 9. The currents without battery smoothing effect (i.e. extracting balance power from battery when enough PV irradiation is not available) and with battery smoothing are respectively presented in Figs. 10 and 11. From the results presented in Figs. 9 through 11 show the operation of the 20

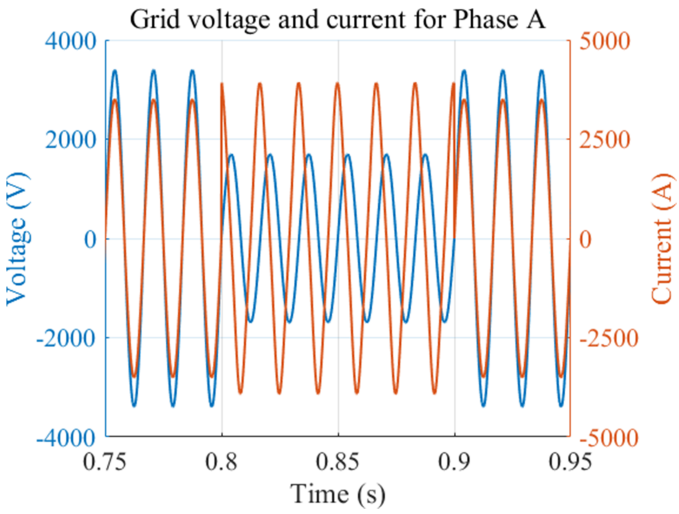

Fig. 12: Grid voltage and current during fault for the faulted phase-a

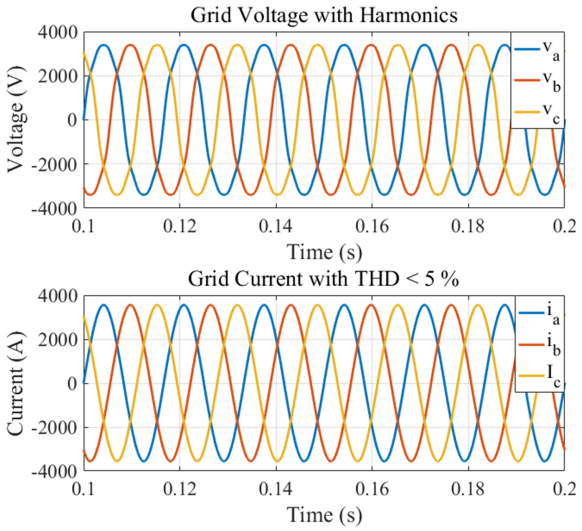

Fig. 13: Grid voltage and current with harmonics

MVA PV farm throughout a day. It is observed from these results that it is possible to meet the objective of supplying commanded power to the grid from the battery when PV irradiation drops. The results showing the operation of the PV farm during an unsymmetrical voltage sag is presented in Fig. 12. In this result, it is shown that during the voltage sag, it is possible to supply reactive power so as to achieve VAr support which is numerically equal to 10 MVAr i.e. nearly 50% of the total system VA rating as per the requirement from [20]. Finally, the result showing transfer of power to the grid in presence of grid harmonics is presented in Fig. 13. With the objective of transferring balanced sinusoidal currents to the grid, the PV farm is capable of transferring low THD sinusoidal currents to the grid even under the presence of grid harmonics.

IV. Conclusion

The simulation of a 20 MVA PV farm for a tri-port MVSI has been presented in this paper. To achieve faster simulation speed, the 25 KVA full switching model is replaced by its equivalent small-signal model and the whole PV farm simulation is accomplished. The comparative results between the full switching model and the corresponding small-signal model are presented to show the possibility to utilize the latter for the farm level study. Various case study results for the PV farm like battery smoothing, reactive power support during unsymmetrical voltage sag and operation during grid harmonics show the efficacy of the overall system under real world PV irradiation profiles. Real time irradiation data for a day are utilized to make the case study scenario more realistic.

References

[1] A. Timbus, M. Liserre, R. Teodorescu, P. Rodriguez, and F. Blaabjerg, "Evaluation of current controllers for distributed power generation systems," *IEEE Transactions on Power Electronics*, vol. 24, pp. 654–664, March 2009.

[2] F. Blaabjerg, R. Teodorescu, M. Liserre, , and A. V. Timbus, "Overview of control and grid synchronization for distributed power generation systems," *IEEE Transactions on Industrial Electronics*, vol. 53, pp. 1398–1409, October 2006.

[3] A. A. Nabulsi and R. Dhaouadi, "Efficiency optimization of a DSP based standalone PV system using fuzzy logic and dual-MPPT control," *IEEE Transactions on Industrial Informatics*, vol. 8, pp. 573–584, Aug 2012.

[4] V. R. Chowdhury and J. W. Kimball, "Control of a three-phase grid-connected inverter under non-ideal grid conditions with online parameter update," *IEEE Transactions on Energy Conversion*, vol. 34, p. 1613–1622, September 2019.

[5] V. R. Chowdhury and J. Kimball, "Grid voltage estimation and feedback linearization based control of a three phase grid connected inverter under unbalanced grid conditions with *lcl* filter," in *Proc. 11th IEEE-ECCE.*, Baltimore, USA, October 2019.

[6] V. R. Chowdhury, R. P. Kandula, and D. Divan, "Lyapunov energy function based control of a soft switching solid state transformer for three-phase standalone application," in *2020 IEEE Energy Conversion Congress and Exposition (ECCE)*, Detroit, MI, USA, October 2020.

[7] V. R. Chowdhury and J. W. Kimball, "Negative virtual capacitance to eliminate resonance oscillations in a three-phase inverter with lcl filter," in *2020 IEEE Energy Conversion Congress and Exposition (ECCE)*, Detroit, MI, USA, October 2020.

[8] U. Datta, A. Kalam, and J. Shi, "Battery energy storage system control for mitigating pv penetration impact on primary frequency control and state-of-charge recovery," *IEEE Transactions on Sustainable Energy*, vol. 11, pp. 746–757, April 2020.

[9] N. Liu, Q. Chen, X. Lu, J. Liu, and J. Zhang, "A charging strategy for pv-based battery switch stations considering service availability and self-consumption of pv energy," *IEEE Transactions on Industrial Electronics*, vol. 62, pp. 4878–4889, August 2015.

[10] Z. An, R. P. Kandula, and D. Divan, "Comparative investigation of system-level optimized power conversion system architectures to reduce lcoe for large-scale pvplus-storage farms," in *2021 IEEE Energy Conversion Congress and Exposition (ECCE)*, Vancouver, Canada, October 2021.

[11] A. Q. Huang, "Medium-voltage solid-state transformer: Technology for a smarter and resilient grid," *IEEE Industrial Electronics Magazine*, vol. 10, pp. 29–42, September 2016.

[12] J. E. Huber and J. W. Kolar, "Solid-state transformers: On the origins and evolution of key concepts," *IEEE Industrial Electronics Magazine*, vol. 10, pp. 19–28, September 2016.

[13] H. Chen and D. Divan, "Design of a 10-kv·a soft-switching solid-state transformer (s4t)," *IEEE Transactions on Power Electronics*, vol. 33, pp. 5724 – 5738, July 2018.

[14] C. Hao and D. Divan, "Soft-switching solid-state transformer (s4t)," *IEEE Transactions on Power Electronics*, vol. 33, pp. 2933 – 2947, April 2018.

[15] L. Zheng, X. Han, Z. An, K. K. Rajendra Prasad Kandula, M. Saeedifard, and D. Divan, "Modular universal converter for mvdc applications," in *2018 IEEE Energy Conversion Congress and Exposition (ECCE)*, Portland, USA, September 2018.

[16] Z. An, R. P. Kandula, and D. Divan, "Feed-forward compensation for model predictive control in tri-port current-source medium-voltage string inverters for pv-plus-storage farms," in *2021 IEEE Energy Conversion Congress and Exposition (ECCE)*, Vancouver, Canada, October 2021.

[17] Z. An, X. Han, L. Zheng, K. Kandasamy, R. P. Kandula, and D. Divan, "Modular isolated soft-switching medium voltage string inverter for large-scale pv farm," in *2020 IEEE Applied Power Electronics Conference and Exposition (APEC)*, New Orleans, LA, USA, February 2020.

[18] NREL, "Nrel, solar irradiation data," https://www.nrel.gov/gis/data-tools.html.

[19] P. Wires and Cables, "Datasheet of cables of various awg," http://www.prioritywire.com/brochures/Utility%20Catalog.pdf.

[20] *IEEE Standard for Interconnecting Distributed Resources with Electric Power systems IEEE Standard 1547a-2014*, pp. 1–16, July 2014.